Analysis of mode-switching of a contra-rotating pump-turbine based on load gradient limiting shutdown and startup sequences

(article starts on next page)

PAPER • OPEN ACCESS

Analysis of mode-switching of a contra-rotating pump-turbine based on load gradient limiting shutdown and startup sequences

View the article online for updates and enhancements.

Analysis of mode-switching of a contra-rotating pump-turbine based on load gradient limiting shutdown and startup sequences

J Fahlbeck[1] ⓘ **, H Nilsson**[1] ⓘ **and S Salehi**[1,2] ⓘ

[1]Department of Mechanics and Maritime Sciences, Chalmers University of Technology, SE-412 96 Gothenburg, Sweden
[2]Chalmers Industriteknik, Gothenburg SE-412 58, Sweden

E-mail: `fahlbeck@chalmers.se`

Abstract. The contra-rotating pump-turbine (CRPT) is investigated as a runner configuration enabling more efficient low-head pumped hydro storage (PHS). To enhance the flexibility of low-head PHS with a CRPT, it is important to examine mode-switching. This study examines two mode-switching sequences for the CRPT, one turbine-to-pump and one pump-to-turbine. The mode-switching sequences are made as a combination of shutdown and startup sequences of each mode. The goal is to avoid pump and turbine brake modes while maintaining smooth load gradients. The turbine shutdown of the turbine-to-pump mode-switching involves a multi-stage valve closure to reduce the rotational speed of the runners, followed by the pump startup based on a previously optimised sequence. The pump shutdown of the pump-to-turbine mode-switching involves a gradual valve closure and rapid speed down of the runners at the end of the sequence. This is followed by the turbine startup, where a valve opens to generate sufficient flow over the runners before increasing the rotational speed of the runners simultaneously. Both mode-switching sequences require approximately 5 s each, and the largest loads are experienced during the pump mode parts of the sequences. The analysis is carried out using transient computational fluid dynamics with the OpenFOAM open-source software.

1. Introduction

The share of renewable energy sources in the electrical grid needs to increase as one effort to reduce global warming [1, 2]. Wind and solar power are the fastest-growing renewable energy sources. To compensate for the intermittency in energy production from these sources, the need for energy storage increases [2, 3].

Pumped hydro storage (PHS) is today the most common form of energy storage [4]. To allow for PHS in regions lacking suitable topography with high mountains, pump-turbine designs intended for low-head energy storage are needed. In the ALPHEUS (augmenting grid stability through low-head pumped hydro energy utilization and storage) EU H2020 project [5, 6], contra-rotating pump-turbines are evaluated as a promising design for low-head PHS [7].

A flexible PHS facility that can react to demand variations from the electrical grid needs to be able to perform fast mode-switching. In one of our previous studies on preliminary startup and shutdown sequences for a CRPT [8], it was observed that during the pump brake mode (see [9] for the working modes of pump-turbines) large and rapid load gradients occurred on the runners. It was suggested that a valve needs to be part of the startup and shutdown sequences. Extensive

studies have been conducted to limit the unfavourable load gradients observed during the pump startup and shutdown sequences of the CRPT [10, 11, 12]. However, investigations of pump-to-turbine and turbine-to-pump mode-switching for the CRPT remain limited. A single study can be found in the literature, by Kanemoto et al. [13], where they conducted an experimental investigation of mode-switching from turbine-to-pump mode of a CRPT. In their study, the rotational speeds of the runners were changed during the sequence, and large torque spikes were identified during the pump braking mode.

In the present study we integrate the previously investigated pump startup and shutdown sequences with newly explored turbine startup and shutdown sequences, forming comprehensive mode-switching sequences. A valve closure/opening plays a key role in limiting the flow rate, thereby avoiding the worst conditions during the sequences. The main purpose of the analysed sequences is to avoid both the pump brake quadrant as well as the turbine braking [9]. The mode-switching sequences are investigated using computational fluid dynamics (CFD) with the OpenFOAM open-source CFD software on the model scale CRPT developed in the ALPHEUS project [14].

2. Geometry and method

The investigated model scale CRPT, along with its mounting arrangement and its conceptual mechanical layout, is shown in Fig. 1a. The full computational domain for the CFD simulations is shown in Fig. 1b. Each of the runners is connected to an individual variable-speed motor-generator unit, allowing the rotational speed of each runner to be controlled independently. Runner 1 is located upstream in pump mode and downstream in turbine mode. Runner 1 has eight blades, while Runner 2 has seven blades. The shroud diameter is 276 mm, and the tip clearance is 0.5 mm. The model scale CRPT corresponds to an experimental test rig for which more details can be found in the work by Hoffstaedt et al. [14].

(a) Geometry, with mounting arrangement and conceptual mechanical layout

(b) Full computational domain, low-pressure boundary to the left and high-pressure to the right
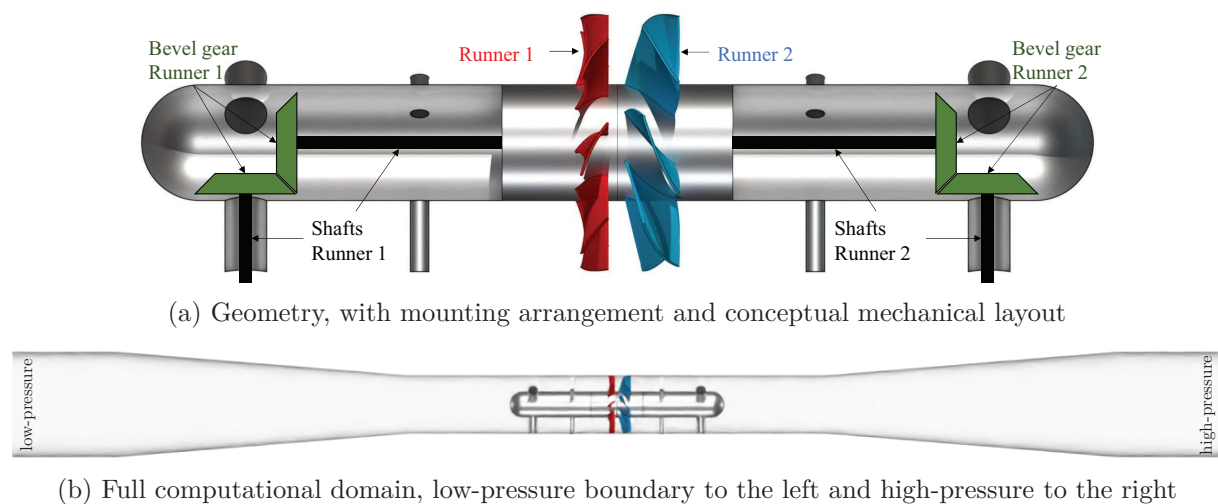
Figure 1. Contra-rotating pump-turbine and computational domain, flow from right to left in turbine mode and left to right in pump mode

2.1. Mode-switching sequences

The selected nominal operating conditions for the CRPT used in this study are found in Table 1, and the investigated mode-switching sequences are shown in Fig. 2. In the sequences, linear functions are used to prescribe the changes in valve opening and runner rotational speeds. Note

32nd IAHR Symposium on Hydraulic Machinery and Systems

IOP Conf. Series: Earth and Environmental Science **1411** (2024) 012049

IOP Publishing

doi:10.1088/1755-1315/1411/1/012049

however that the transitions between the linear functions are smoothed to replicate the time required for these transitions to take place. This consideration is furthermore crucial because sudden changes can lead to pressure spikes due to the assumption of incompressible flow in the simulations. In the evaluated sequences, the goal is to avoid both the pump brake quadrant and the turbine braking of a pump-turbine's operating modes [9].

In the turbine-to-pump mode-switching (Fig. 2a), the turbine shutdown occurs during 0–1.50 s and the pump mode startup occurs during 1.70–4.95 s. In the turbine shutdown, a multi-stage valve closure is assumed. This approach is favourable as it allows for a decreased flow rate as the runners gradually decelerate, thereby mitigating the runner loads during the sequence. In the sequence, Runner 2 begins to slow down before Runner 1, and both runners come to a complete stop before the valve is fully closed. This is because the motor-generator unit should not need to add torque to keep the runners rotating, thus avoiding the runaway condition and turbine brake mode. For the pump startup, the runner rotational speeds initially increase so that the net head matches the gross head. This means the pump brake quadrant is avoided. After the initial acceleration of the runner speeds, the optimised pump startup sequence from our earlier work is applied [11]. However, here the aforementioned modifications using linear functions instead of sinusoidal functions are used, and the nominal operating conditions have been altered due to constraints from the test facility.

Table 1. Selected nominal operating conditions of the CRPT

	Turbine mode	Pump mode	
Runner 1 rotational speed (n_{R1})	842	1250	rpm
Runner 2 rotational speed (n_{R2})	633	1125	rpm
Power (P)	13.8	38.5	kW
Flow rate (Q)	270	345	l/s
Net head[a] (H)	5.8	10.1	m
Hydraulic efficiency[b] (η)	89.9	88.3	%
Specific speed[c] (Ω_s)	3.9	4.7	-

[a] Calculated by the total pressure change over the runners
[b] Based on the net head of the CRPT
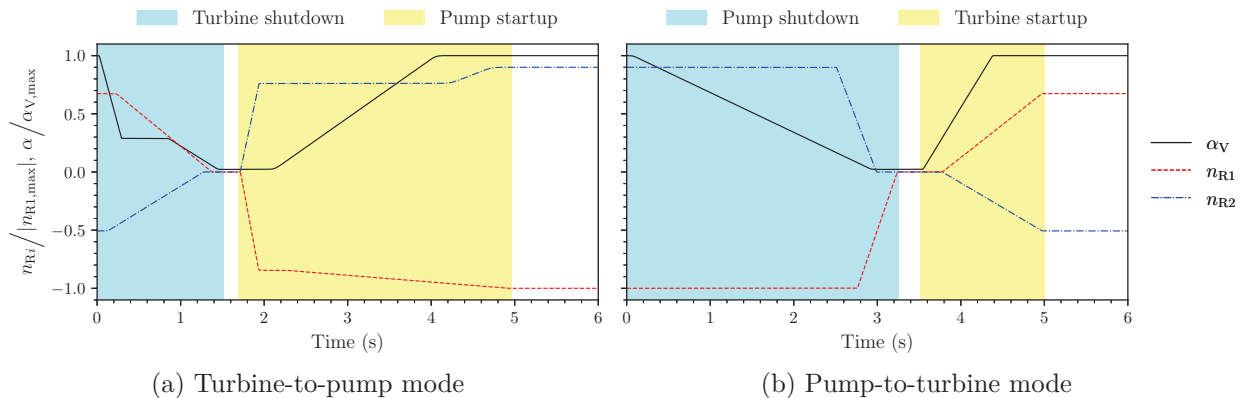[c] Based on the runners relative angular velocity in rad/s through Eq. (2) from [7]

(a) Turbine-to-pump mode

(b) Pump-to-turbine mode

Figure 2. Mode-switching sequences, where α_V is the valve, n_{R1} and n_{R2} are the Runner 1 and 2 rotational speeds, respectively

For the pump-to-turbine mode-switching (Fig. 2b), the pump shutdown occurs during 0–3.25 s, and the turbine startup occurs during 3.50–5.00 s. For the pump shutdown, it has been shown that it is preferable to close the valve before decelerating the runners [12]. This is why the valve is nearly fully closed before the runners begin to speed down. Runner 1 starts decelerating after Runner 2, as this helps to avoid reverse flow in the final parts of the sequence. The turbine startup begins by opening the valve to ensure an adequate flow before starting to increase the rotational speed of the runners. During the turbine startup, the time-variation of the runner loads is marginally improved by accelerating the runners simultaneously, as opposed to letting one of the runners start to speed up before the other.

2.2. Numerical set-up
The incompressible Reynolds-averaged Navier-Stokes equations are discretised and solved on the computational mesh with the OpenFOAM-v2112 open-source CFD code. For closure and to account for turbulence, the k-ω SST-SAS [15] (shear stress transport - scale adaptive simulation) model is used. Several recent studies have given confidence that this turbulence model can accurately predict the flow field for hydro turbines [16, 17].

The discretisation of the convection terms of the three momentum equations employs the second-order accurate linear upwind stabilised transport (LUST) scheme [18]. Meanwhile, the turbulent quantities k and ω are discretised using the first-order accurate upwind scheme. The remaining terms are discretised with the second-order accurate central difference scheme. Time derivatives are handled using the second-order backward scheme [19]. A constant time step of 5×10^{-5} s is used, equivalent to a maximum runner rotation of $0.38°$ per time step.

The mesh is divided into four parts, one for each of the runners and the two domains that are located before and after the CRPT. The arbitrary mesh interface [20] technique is used to transfer fluxes at the sliding interfaces connecting the mesh regions. The total cell count of the mesh is around 16.6×10^6 cells. Each of the runner regions has about 4.3×10^6 cells, and the two parts upstream and downstream consist of around 4×10^6 cells each.

The `headLossPressure` boundary condition [21] is used at the low-pressure and high-pressure boundaries (see Fig. 1b) of the numerical domain to achieve a flow-driving pressure difference. The boundary condition is configured to account for the components that are not part of the numerical domain by prescribing head losses according to the lab test facility. The valve sequence is controlled as a time-varying head loss at the high-pressure boundary through the local loss coefficient (k_V) of the valve at various opening angles (α_V) as

$$k_V(\alpha_V) = \exp(-4.2351 \ln(\alpha_V) + 18.1149). \tag{1}$$

This is because the valve is located on the high-pressure side of the CRPT. A valve opening of $90°$ represents the fully open state and $0°$ fully closed. In the simulations, the smallest possible valve opening is $2°$ because of the logarithmic function in Eq. (1).

The input data for the `headLossPressure` boundary condition is shown in Table 2. The 'Sharp exit' and 'Sharp entrance' remain unchanged as the flow rate changes direction during mode-switching. This is because of the fact that in the incompressible `pimpleFoam` solver, the specific pressure level does not influence the outcome. The pressure difference remains constant regardless of whether a loss is specified at the low- or high-pressure boundary as long as the total losses remain unchanged.

3. Results and discussion
The results for the turbine-to-pump mode-switching are presented in Section 3.1, followed by the results for the pump-to-turbine mode-switching in Section 3.2. However, before analysing the mode-switching, the flow field at the nominal operating conditions in Fig. 3 is first discussed.

32nd IAHR Symposium on Hydraulic Machinery and Systems

IOP Publishing

IOP Conf. Series: Earth and Environmental Science **1411** (2024) 012049

doi:10.1088/1755-1315/1411/1/012049

Table 2. Input to the pressure boundary condition at the low- and high-pressure boundaries

	low-pressure	high-pressure	
Surface elevation	2.25	9.70	m
Local losses (loss coefficient)			
Bend	–	0.20	–
Sharp entrance	–	0.45	–
Sharp exit	1.00	–	–
Fixed valve	–	0.40	–
Flow control valve, Eq. (1)	–	$k_V(\alpha_V, t)$	–
Friction losses			
Pipe length	1.00	15.05	m
Surface roughness	0.05	0.05	mm

(a) Turbine mode at the nominal operating condition

(b) Pump mode at the nominal operating condition

(c) CRPT precisely counteracting the gross head, yielding zero through-flow
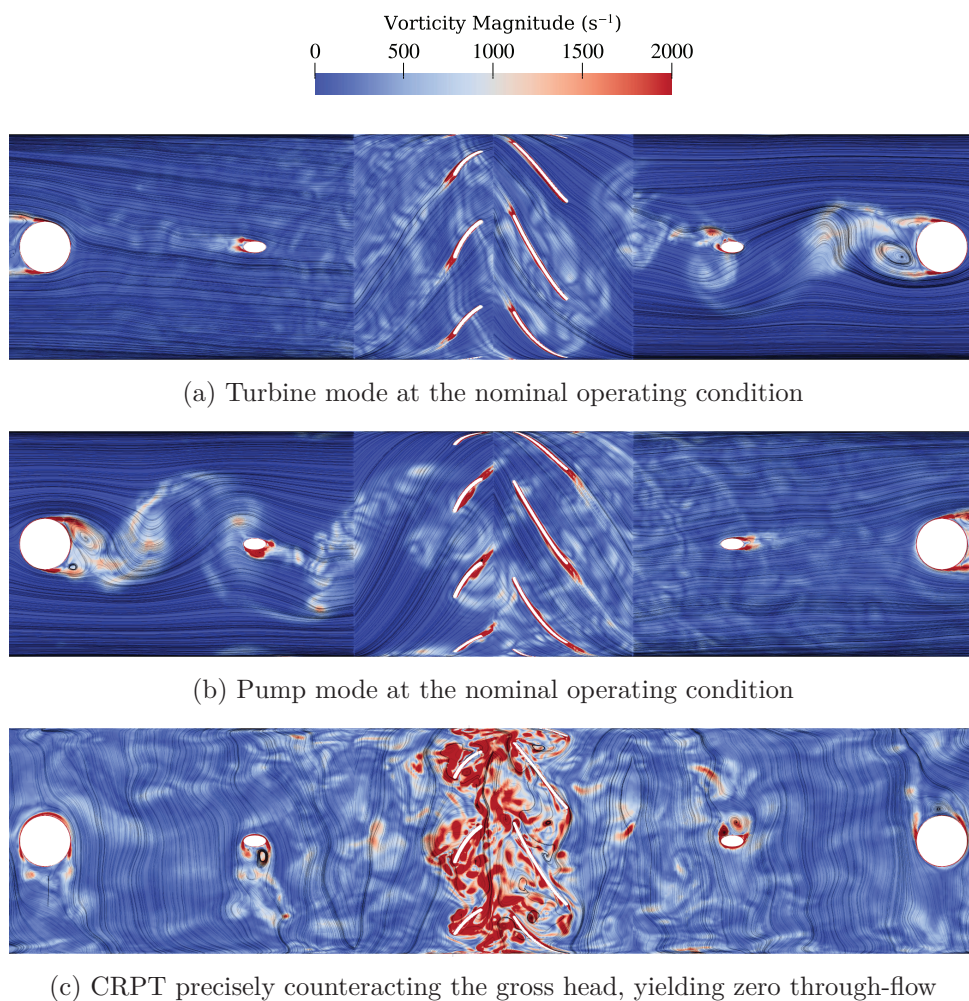
Figure 3. Snapshots of vorticity magnitude and streamlines of the relative velocity on a cylindrical cut of the CRPT

Figure 3 shows the vorticity magnitude and streamlines of the relative velocity at the nominal turbine mode (Fig. 3a), the nominal pump mode (Fig. 3b), and when the runners precisely counteract the gross head and give a zero flow through the CRPT (Fig. 3c). In both turbine and pump modes, the incoming and outgoing flow primarily occur in the axial direction, indicating high machine efficiency. However, von Kármán vortices are generated because of flow separation from the upstream support struts. Additionally, complex vortical structures are developed in the blade passages of the downstream runner as a result of the interactions between the blades, which are transported downstream of the CRPT. At the zero through-flow condition, the flow in the blade passages is very complex, as in a mixer, and the streamlines show strong contra-swirling flows at the sides of the CRPT.

3.1. Turbine-to-pump mode-switching

Figure 4 shows the time-evolution of the computed flow rate (left), the runner axial forces (middle) and the runner torques (right) for the turbine-to-pump mode-switching. At the start of the turbine shutdown, the runner loads are initially decreasing with the decreasing flow rate. However, during the period when the valve opening remains at the plateau (0.3–0.8 s), there is a marginal increase in the runner loads. This phenomenon arises as a consequence of the diminishing rotational speed, resulting in the runners blocking the flow rather than efficiently directing it. Subsequently, as the valve closure commences and the rotational speed of the runners approaches the standstill, the loads rapidly diminish to zero. Through this turbine shutdown sequence, negative torque is prevented because the rotational speed is maintained below the runaway speed at all times.

During the pump startup phase (after 1.5 s), the flow rate is unaffected by the initial fast increase of the runner rotational speeds. However, the loads rapidly increase with the acceleration of the runners. At this stage, the runners are mainly mixing the flow (see Fig. 3c for a visual representation of the flow field as the runners work as mixers) as no through-flow can be generated because of the closed valve and the rotational speed being set in such way that the net head matches the gross head. The flow rate and runner loads are starting to change at around 3.5 s. The flow rate increases in the pump mode direction (indicated by the negative value) as the valve opens (2.00–4.18 s) and the Runner 1 rotational speed increases (2.22–4.95 s). The Runner 1 loads are practically constant between 2.0–4.6 s. Thereafter, the loads first decrease, then increase at around 5 s, before finally reaching the nominal load conditions. This is in contrast to the Runner 2 loads, which undergo an increase between around 3.8–5.1 s. The initial increase in the Runner 2 loads is because of the increasing flow rate as Runner 1 increases its rotational speed. After the Runner 2 load peak, the loads rapidly decrease to the nominal operating conditions.
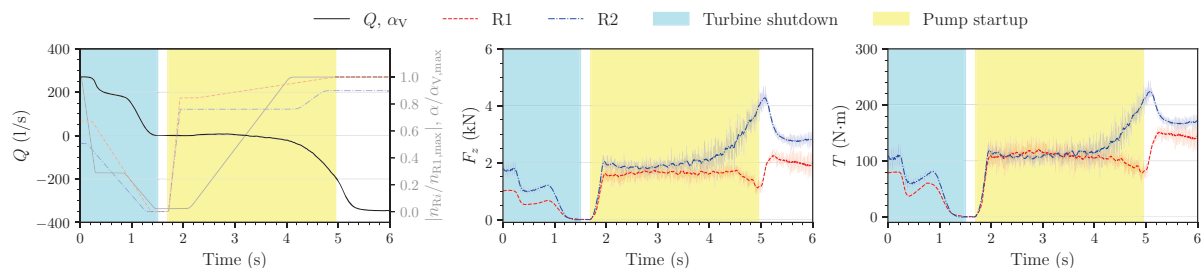

Figure 4. Flow rate and sequence as shaded (left), runner axial force (middle) and runner torque (right) during the turbine-to-pump mode-switching. R1 and R2 denote Runner 1 and Runner 2, respectively.

32nd IAHR Symposium on Hydraulic Machinery and Systems

IOP Publishing

IOP Conf. Series: Earth and Environmental Science **1411** (2024) 012049

doi:10.1088/1755-1315/1411/1/012049

The Runner 2 load peak at around 5.1 s is predominantly a consequence of the increasing flow rate. This is demonstrated by the velocity triangles in Fig. 5. Between 4.9–5.3 s the flow rate is almost doubled, as indicated by the enlargement of the axial component (u_z). At 4.9 s (left in Fig. 5), Runner 1 is mostly mixing the flow as its upstream and downstream velocity triangles are practically identical. At the same time, Runner 2 is responsible for generating most of the work added to the flow, as shown by the difference in tangential velocity (u_θ) over the runner. At 5.1 s (middle in Fig. 5), Runner 1 is starting to work more as a pump. This is indicated by the incoming absolute velocity being more aligned with the axial direction and the deceleration of the relative velocity (u_{rel}) over the runner. This is the reason why the loads increase for Runner 1 at 5.1 s. The magnitude of the tangential component of the incoming flow for Runner 2 is practically the same as at 4.9 s. However, both the incoming absolute and relative flow angles are decreased because of the increased axial velocity. The change of tangential velocity over Runner 2 slightly reduces between 4.9 and 5.1 s. Still, the axial velocity increases more than the change of tangential velocity is reduced, which explains the higher runner loads at 5.1 s. To the right in Fig. 5, the velocity triangles are shown at 5.3 s, shortly after the load peak. The axial velocity has further increased, and the incoming absolute flow for Runner 1 is almost entirely in the axial direction. This results in the incoming flow angles for Runner 2 being reduced. Likewise, the change of tangential velocity over Runner 2 is drastically reduced compared to at 4.9 and 5.1 s, which explains the decreasing loads at this time in Fig. 4.
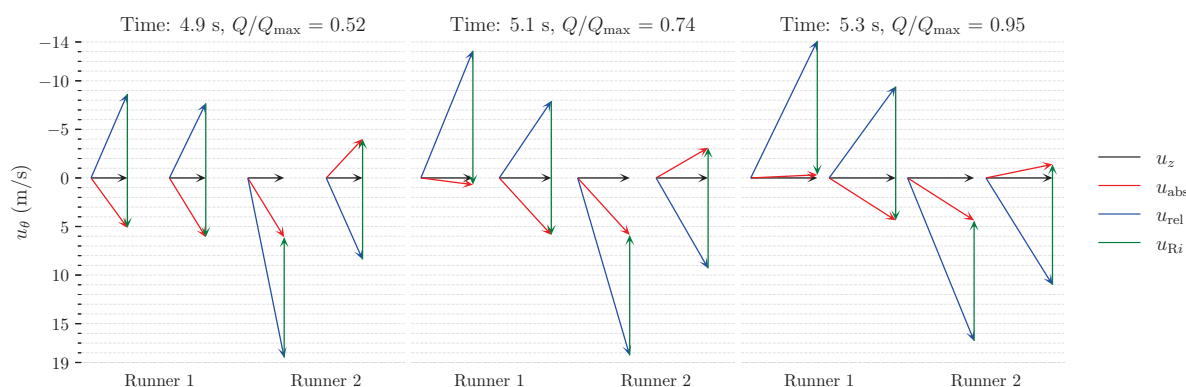

Figure 5. Snapshots of spatially averaged velocity triangles close to the load peak during the pump startup of the turbine-to-pump mode-switching. For each runner, the left triangle indicates the incoming and the right the outgoing flow, respectively.

Note that the increase in the Runner 2 loads, surpassing those at the final operating condition, was not observed in the optimised sequence outlined in our earlier work [11]. This discrepancy arises from the nearly 16% increase in gross head and the reduction in nominal pump mode rotational speed of the runners in this study compared to the previous one. Additionally, the sinusoidal functions employed in the prior study resulted in smoother transitions in the rotational speed and thus potentially also the runner loads.

3.2. Pump-to-turbine mode-switching

Figure 6 shows the time-evolution of the flow rate (left), the runner axial forces (middle) and the runner torques (right) for the pump-to-turbine mode-switching. During the pump shutdown, the flow rate is stable before approximately 1 s, whereafter it starts to rapidly decrease as the valve closes further. After around 2.8 s, there is a negligible amount of remaining flow rate as the valve is almost fully closed. As the flow rate decreases, the Runner 2 axial force and
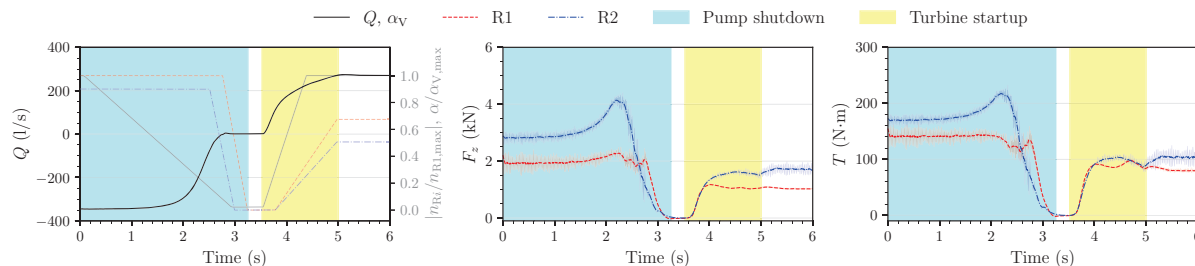
32nd IAHR Symposium on Hydraulic Machinery and Systems

IOP Publishing

IOP Conf. Series: Earth and Environmental Science **1411** (2024) 012049

doi:10.1088/1755-1315/1411/1/012049

Figure 6. Flow rate and sequence as shaded (left), runner axial force (middle) and runner torque (right) during the pump-to-turbine mode-switching. R1 and R2 denote Runner 1 and Runner 2, respectively.

torque increase, reaching peak values at 2.2–2.3 s. At the same time, the Runner 1 loads are comparably stable. The Runner 2 load peak occurs before the rotational speed of the runners starts to decrease. It is thus an effect of the decreasing flow rate as the valve closes. To illustrate what the flow field undergoes at the Runner 2 load peak, Fig. 7 shows a zoom of the vorticity magnitude and streamlines of the relative velocity at a cylindrical cut of the CRPT (left) and spatially averaged incoming velocity triangles for Runner 2 (right). As the flow rate decreases, the upstream Runner 1 cannot effectively guide the flow towards the downstream Runner 2. This results in flow separation on the suction side of the Runner 1 blades, which affects the flow approaching Runner 2. Furthermore, as an effect of the decreasing flow rate, while the runners still rotate at their nominal speed, the absolute flow angle leaving Runner 1 increases. This results in a significant increase in the incoming relative flow angle for Runner 2, leading to extensive flow separation along the suction side of its blades, as depicted in Fig. 7b. After the Runner 2 load peak at 2.5 s, the runners are mainly mixing the flow as shown by the extensive separation observed throughout the entire Runner 2 blade passages in Fig. 7c. As the valve continues to close and the runners are brought to a standstill, the flow rate and loads on the runners rapidly reduce to zero.

Focusing on the turbine startup shown in Fig. 6, the flow rate and runner loads increase as the valve opens to allow flow over the runner blades. The rapid initial rise in the loads on the runners, before 4 s, is an effect of the accelerating flow rate since the runners have barely started to increase their rotational speeds. After 4 s, the rotational speed of the runners increases further, and the flow rate continues to rise as the runners effectively guide the flow through the blade passages. After the sequence, an extra time of approximately 0.3 s is needed for the runner loads to settle at the final operating condition. Negative torque is avoided through the sequence since a sufficient flow is developed before starting to speed up the runners.

4. Conclusions

Mode-switching sequences of a model-scale CRPT were investigated with CFD in this study. The mode-switching sequences were based on load gradient limiting startup and shutdown sequences of each mode. These were merged to create full turbine-to-pump and pump-to-turbine mode-switching sequences. In these sequences, a valve was assumed to control the flow rate, and the rotational speed of the runners were varied between the nominal operating condition and standstill. The duration of the evaluated turbine-to-pump mode-switching sequence was 4.95 s, and the pump-to-turbine mode-switching sequence lasted 5.00 s.

In the turbine shutdown of the turbine-to-pump mode-switching, a multi-stage valve closure was implemented to limit the flow rate as the runners were brought to a standstill. The load variation on the runners during the turbine shutdown was comparably smooth in contrast to
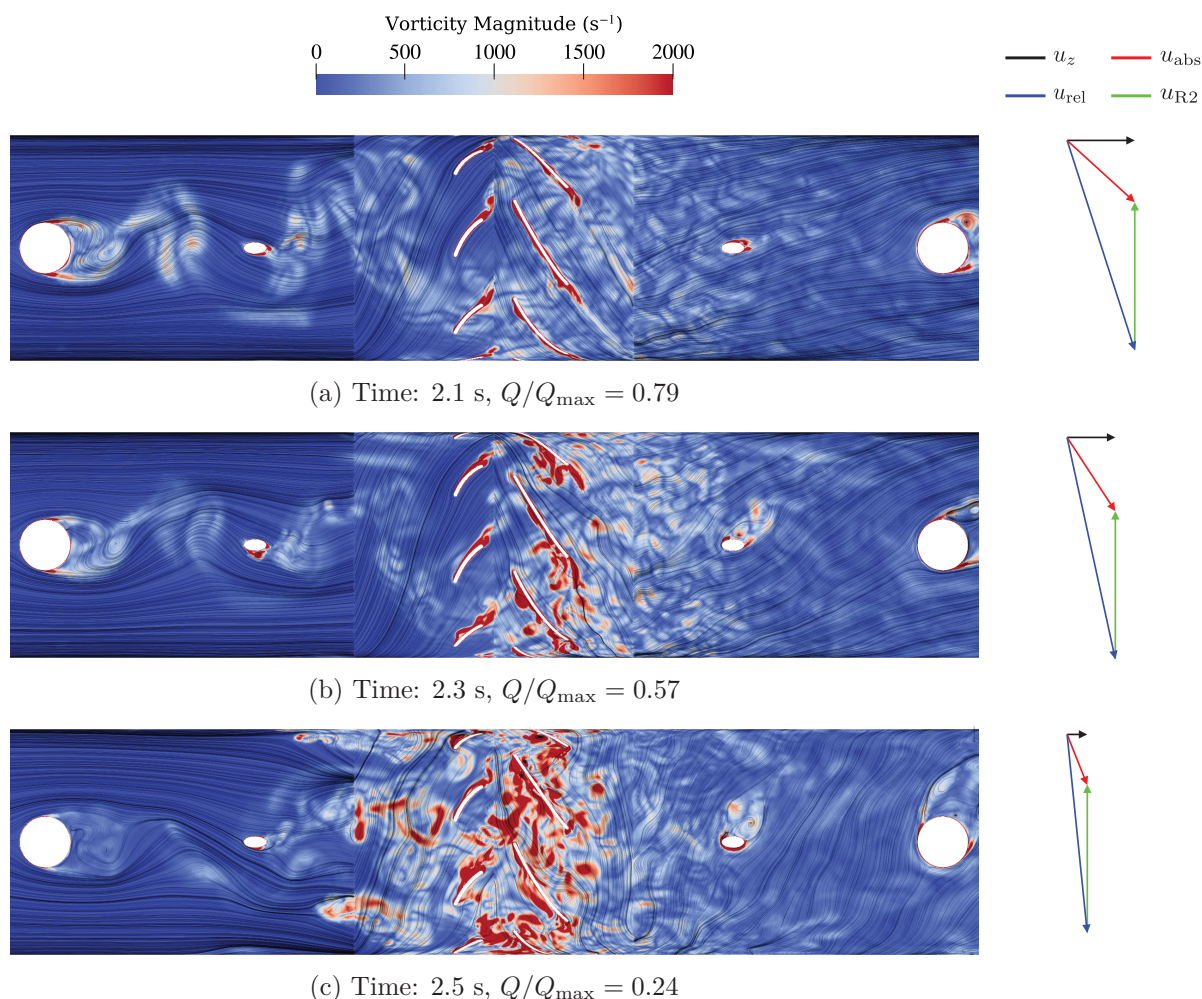
(a) Time: 2.1 s, $Q/Q_{\max} = 0.79$

(b) Time: 2.3 s, $Q/Q_{\max} = 0.57$

(c) Time: 2.5 s, $Q/Q_{\max} = 0.24$

Figure 7. Snapshots of vorticity magnitude and streamlines of the relative velocity on a cylindrical cut of the CRPT (left), and incoming velocity triangles for Runner 2 (right), at times close to the Runner 2 load peak at the pump mode shutdown during the pump-to-turbine mode-switching

the pump startup. During pump startup, the runners were initially accelerated with a fully closed valve to ensure that the CRPT net head matched the gross head. Thereby preventing the pump brake mode and reversed flow during the sequence. For the remainder of the sequence, a previously optimised pump startup sequence was applied. However, variations existed as the nominal operating conditions were altered in this study compared to the previous. These differences led to a load peak for Runner 2, surpassing the loads at the final operating condition. This suggests that the nominal operating conditions play an important role in the load gradients during the pump startup sequence.

In the pump shutdown phase of the pump-to-turbine mode-switching, the valve was fully closed before the runners reached the standstill position. This ensured that reversed flow was avoided during the pump shutdown. Similar to the pump startup, a load peak occurred for Runner 2 during the pump shutdown. The load peak was caused by the decelerating flow rate, leading to unsteady flow separation from Runner 1 as well as an increasing incoming relative flow angle for Runner 2. This resulted in massive flow separation, primarily on the suction side of the Runner 2 blades. Despite this, the Runner 2 load increase demonstrated smooth

behaviour without any spikes. During the turbine startup, the runner loads rapidly increased as the flow rate accelerated because of the opening valve. Subsequently, as the rotational speed of the runners increased, the flow rate continued to rise as the runners effectively guided the flow through the blade passages. In the turbine startup sequence, negative torque and high amplitude loads were avoided by starting to speed up the runners simultaneously as the valve opened up.

A further step would be to explore how and why the nominal conditions impact the peak runner loads observed during the sequences. This is because the present study demonstrated larger runner loads compared to our previous work despite employing similar sequences. Another aspect would be to examine the sequences from this study at a prototype scale CRPT. Conducting such a study could offer insights into the scalability of the sequences, potentially leading to an understanding of how to execute mode-switching for enhanced flexibility in future low-head PHS facilities with CRPTs.

Acknowledgement

References

[1] IRENA 2020 *Global Renewables Outlook: Energy Transformation 2050* (International Renewable Energy Agency (IRENA)) ISBN 978-92-9260-238-3

[2] IRENA 2024 *Tracking COP28 outcomes: Tripling renewable power capacity by 2030* (Abu Dhabi: International Renewable Energy Agency) ISBN 978-92-9260-585-8

[3] IEA 2023 *Net Zero Roadmap: A Global Pathway to Keep the 1.5 °C Goal in Reach* (Paris: IEA) URL `https://www.iea.org/reports/net-zero-roadmap-a-global-pathway-to-keep-the-15-0c-goal-in-reach`

[4] Murdock H E *et al.* 2021 Renewables 2021 - Global status report Tech. Rep. 978-3-948393-03-8 REN21 France iNIS–FR–21-0788

[5] 2024 ALPHEUS H2020 URL `https://alpheus-h2020.eu/` accessed on 03 April 2024

[6] Qudaih M *et al.* 2020 The Contribution of Low-Head Pumped Hydro Storage to a successful Energy Transition *Proceedings of the Virtual 19th Wind Integration Workshop*

[7] Hoffstaedt J P *et al.* 2022 *Renewable and Sustainable Energy Reviews* **158** 112119 ISSN 1364-0321

[8] Fahlbeck J, Nilsson H and Salehi S 2021 *Energies* **14** 3593 ISSN 1996-1073

[9] Cavazzini G *et al.* 2018 *Renewable and Sustainable Energy Reviews* **94** 399–409 ISSN 1364-0321

[10] Fahlbeck J, Nilsson H and Salehi S 2022 *IOP Conf Ser Earth Environ Sci* **1079** 012034 ISSN 1755-1315

[11] Fahlbeck J, Nilsson H and Salehi S 2023 *Journal of Energy Storage* **62** 106902 ISSN 2352-152X

[12] Fahlbeck J, Nilsson H and Salehi S 2023 On the pump mode shutdown sequence for a model contra-rotating pump-turbine *Under Review* (Romania, Timisoara)

[13] Kanemoto T, Honda H, Kasahara R and Miyaji T 2014 *IOP Conf Ser Earth Environ Sci* **22** 012032 ISSN 1755-1315

[14] Hoffstaedt J P *et al.* 2023 Experimental setup and methods for a novel low-head pumped storage system *IET Conference Proceedings* vol 7 (IET Digital Library) pp 341–348

[15] Egorov Y and Menter F 2008 Development and Application of SST-SAS Turbulence Model in the DESIDER Project *Advances in Hybrid RANS-LES Modelling* (Springer) pp 261–270 ISBN 978-3-540-77815-8

[16] Sotoudeh N, Maddahian R and Cervantes M J 2020 *Renewable Energy* **151** 238–254 ISSN 0960-1481

[17] Salehi S, Nilsson H, Lillberg E and Edh N 2021 *Renewable Energy* **179** 2322–2347 ISSN 0960-1481

[18] Weller H 2012 *Monthly Weather Review* **140** 3220–3234 ISSN 1520-0493, 0027-0644

[19] Jasak H 1996 *Error analysis and estimation for the finite volume method with applications to fluid flows.* (Imperial College London (University of London))

[20] Aguerre H J *et al.* 2017 *Journal of Computational Physics* **335** 21–49 ISSN 0021-9991

[21] Fahlbeck J, Nilsson H and Salehi S 2022 *OpenFOAM Journal* **2** 1–12 ISSN 2753-8168